Accepted Manuscript

http://dx.doi.org/10.1002/chem.201800980

M. Mangstl, J. Weber, D. Jardón Álvarez, O. Burghaus, B. Roling, and J. Schmedt auf der Günne. Investigation of bistetramethylammonium hydrogencyclotriphosphate - a molecular rotor? *Chem. - Eur. J.*, 24:8756--8759, 2018.

Investigation of bistetramethylammonium hydrogencyclotriphosphate – a molecular rotor?**

Martin Mangstl,[a] Johannes Weber,[a] Daniel Jardón-Álvarez,[b] Olaf Burghaus,[c] Bernhard Roling[c] and Jörn Schmedt auf der Günne*[a]

Abstract: The crystalline phase β-$[N(CH_3)_4]_2HP_3O_9$ undergoes a reversible phase transition to γ-$[N(CH_3)_4]_2HP_3O_9$, which was studied by dynamic scanning calorimetry and X-ray diffraction. The rotational dynamics of the anion $[P_3O_9]^{3-}$ were evident from variable temperature ^{31}P MAS NMR spectroscopy. The rotational dynamics could be simulated with a 3-site jump model, which yields spectra in good agreement with experiment. An activation energy of 0.6 eV could be estimated from line shape analysis. Impedance spectra reflect a bulk proton conductivity of γ-$[N(CH_3)_4]_2HP_3O_9$ of $6.9 \cdot 10^{-5}$ S/cm at 240 °C and an activation energy of approximately 1.0 eV. Thus this salt features bulk protonic motion while local rotational anionic motion happens with activation energies of the same order, as suggested by the paddle wheel mechanism.

Protonic conductors are mainly used for fuel cells, sensor applications and hydrogen separation.[1–4] Thereby phosphate-based compounds are interesting because of their low cost of production and relatively low toxicity. Among many different phosphate-based protonic conductors the following are promising candidates: RbH_2PO_4,[5] CsH_2PO_4,[6] $Mn(H_2PO_4)_2$,[7] α-$Zr(HPO_4)_2$[8] and γ-$Zr(PO_4)(H_2PO_4)\cdot 2H_2O$.[9] Especially CsH_2PO_4 is under investigation due to the intermediate operating temperature range (200–300 °C) under relatively dry conditions, showing a high conductivity of $2.2 \cdot 10^{-2}$ S/cm at 240 °C.[6] This allows the production of cheaper membranes than the Nafion[10] based ones due to the possibility of using cheaper catalysts than platinum. Furthermore this temperature window is interesting for sensor applications because it allows the detection of species towards which the sensors are inert at lower temperatures.

In general high ionic conductivities can be expected for systems with relatively big cations due to lower Coulomb interaction between anions and cations. Thus bigger cations than Cs^+ like the tetramethylammonium cation are desirable. From literature only the tetramethylammonium orthophosphates $[N(CH_3)_4]H_2PO_4 \cdot 0.5\ H_2O$,[11] $[N(CH_3)_4]H_2PO_4 \cdot H_2O$[12] and the metaphosphates α- and β-$[N(CH_3)_4]_2HP_3O_9$ which contain the more bulky anion $P_3O_9^{3-}$ are known.[13,14]

For the conduction mechanism of high temperature ionic conductors two different mechanisms are discussed in literature. Some authors try to explain the high temperature conductivity with a percolation-type mechanism.[15,16] Other authors claim that the paddle-wheel mechanism within so called rotator phases is responsible for the increased ion conductivity in certain high temperature ion conductors, e.g. for CsH_2PO_4.[17–19] Moreover big molecular rotors are used as mechanical elements for molecular machines.[20–22]

In this article we investigate the phase transition of β-bistetramethylammonium hydrogencyclotriphosphate to a phase which features molecular dynamics at elevated temperatures by means of differential scanning calorimetry (DSC), impedance spectroscopy, variable temperature powder X-ray diffraction and variable temperature solid state nuclear magnetic resonance (NMR).

In order to identify the nature and temperature of appearing phase transitions DSC measurements were performed. The as prepared sample of α-$[N(CH_3)_4]_2HP_3O_9$ shows an irreversible first order phase transition to β-$[N(CH_3)_4]_2HP_3O_9$ with an onset temperature of 195 °C.[14] If β-$[N(CH_3)_4]_2HP_3O_9$ is heated up to higher temperatures a reversible phase transition to γ-$[N(CH_3)_4]_2HP_3O_9$ can be observed (Figure 1).

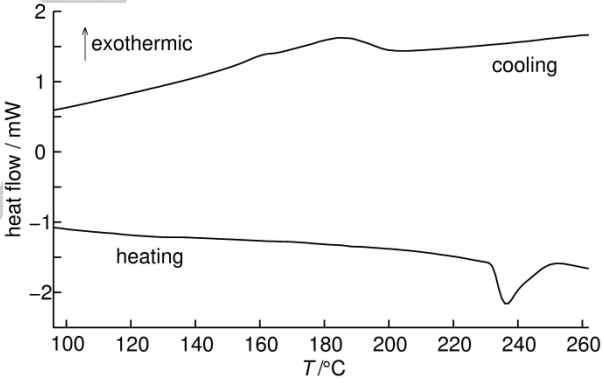

Figure 1. DSC measurement of β-$[N(CH_3)_4]_2HP_3O_9$ between 98 and 262 °C with a heating/cooling rate of 5 K/min (heating: lower line, cooling: upper line). Onset temperature of a reversible phase transition during heating at 232°C and during cooling at 206 °C.

By integration of the signal within a background corrected heating curve the following reaction enthalpies can be estimated:

$$\beta\text{-}[N(CH_3)_4]_2HP_3O_9 \rightarrow \gamma\text{-}[N(CH_3)_4]_2HP_3O_9 \quad \Delta_{Tra}H = +3.56\ \text{kJ / mol}$$

$$\gamma\text{-}[N(CH_3)_4]_2HP_3O_9 \rightarrow \beta\text{-}[N(CH_3)_4]_2HP_3O_9 \quad \Delta_{Tra}H = -3.53\ \text{kJ / mol}$$

Moreover powder X-ray diffraction measurements at various temperatures during heating and cooling were carried out for analyzing the thermal behavior on a macroscopic scale. During heating a phase transition of phase α into β takes place at approximately 152 °C (Figure 2). The β-phase undergoes a phase transition into the γ-phase at approximately 230 °C.

[*] Prof. Dr. J. Schmedt auf der Günne
E-mail: gunnej@chemie.uni-siegen.de
[a] Inorganic Materials Chemistry
Universität Siegen
Adolf-Reichwein-Straße 2, 57076 Siegen, Germany
[b] Inorganic Chemistry,
Universität München
Butenandtstraße 5-13, D-81377 Munich, Germany
[c] Physical Chemistry
Philipps-Universität Marburg
Hans-Meerwein-Str. 4, 35032 Marburg, Germany

[**] We want to thank Dr. Christian Pritzel for the help with DSC measurements.

Supporting information for this article is given via a link at the end of the document.

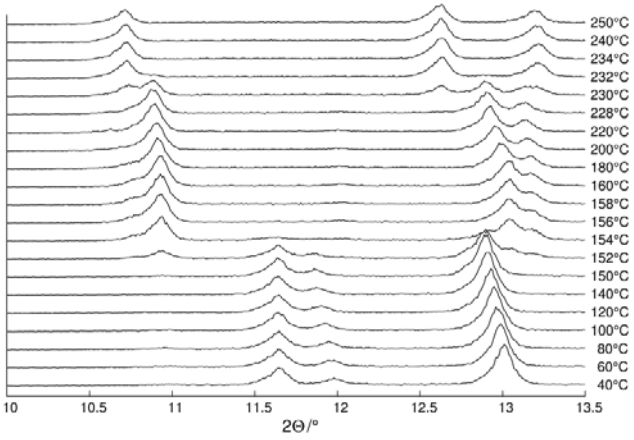

Figure 2. Observed powder diffraction patterns of initially α-$[N(CH_3)_4]_2HP_3O_9$ measured with $CuK_{\alpha 1}$ radiation at variable temperatures during first heating run.

During cooling the phase transition of the γ-phase into the β-phase happens at approximately 210 °C (Figure S2). However no phase transition from phase β into phase α can be observed which means that phase β is the thermodynamic stable phase. Exactly the same experiments were done for a second time directly after the first run (Figure S3). Again a phase transition of phase β into phase γ can be observed at the same temperature than for the first heating run. This also can be applied for the cooling behavior of the sample which denotes that this process is reversible (Figure S4).

The powder diffraction pattern of γ-$[N(CH_3)_4]_2HP_3O_9$ could be indexed by using the program FOX.[23] The Le Bail fit for a monoclinic unit cell (a = 11.4339 Å, b = 9.2719 Å, c = 17.5704 Å, α = 90 °, β = 90.133 °, γ = 90 °) was in good agreement with the experimental data. The value for the cell volume of γ-$[N(CH_3)_4]_2HP_3O_9$ increased by approximately 6% compared to β-$[N(CH_3)_4]_2HP_3O_9$. Due to low resolution of the measured powder diffraction pattern caused by the high temperature setup it was not possible to identify the space-group of γ-$[N(CH_3)_4]_2HP_3O_9$ unambiguously.

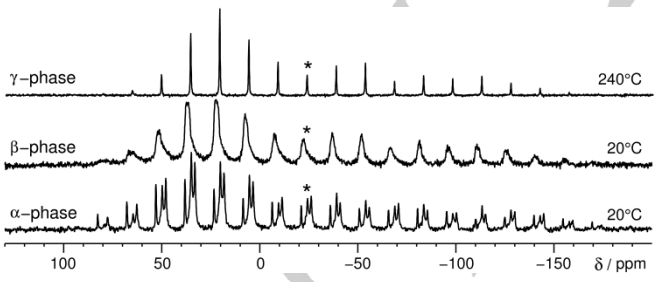

Figure 3. $^{31}P\{^1H\}$ CP-RAMP MAS NMR spectra of α-$[N(CH_3)_4]_2HP_3O_9$ recorded at 20 °C before heating. Phase γ was measured at 240 °C and phase β after heating to 240 °C and subsequent cooling. The spectra include all rotational sidebands, isotropic shifts are signed with an asterisk (spinning frequency: 3 kHz).

Furthermore variable temperature NMR measurements were performed in order to analyze the thermal behavior on a microscopic scale. The spectra presented in Figure 3 show the appearance of three different phases during heating to 240 °C and subsequent cooling to 20 °C. This is in agreement with the phase transitions identified by DSC and variable temperature XRD measurements.

Due to the presence of rotational sidebands in all three phases it can be concluded that solid crystalline phases are present within the complete temperature range of 20 and 240 °C. The obtained results are summarized in Table 1.

Table 1: Chemical shift parameters obtained by fitting the experimental spectra with SIMPSON[24] assuming a single spin system at 20 and 240 °C during heating and at 20 °C after cooling:

	peak	δ_{iso} / ppm	δ_{aniso} / ppm	η	δ_{11} ppm	δ_{22} / ppm	δ_{33} / ppm
α-phase (20 °C)	1	−21.5	−168	0.3	87.7	37.3	−189.5
	2	−24.6	−146	0.2	63.0	33.8	−170.6
	3	−26.5	−152	0.3	72.3	26.7	−178.5
β-phase (20 °C)	1	−21.1	−142	0.0	48.9	48.9	−164.1
	2	−23.7	−122	0.4	61.7	12.9	−145.7
	3	−24.4	−172	0.3	87.4	35.8	−196.4
γ-phase (240 °C)	1	−24.4	−172	0.3	87.4	35.8	−196.4

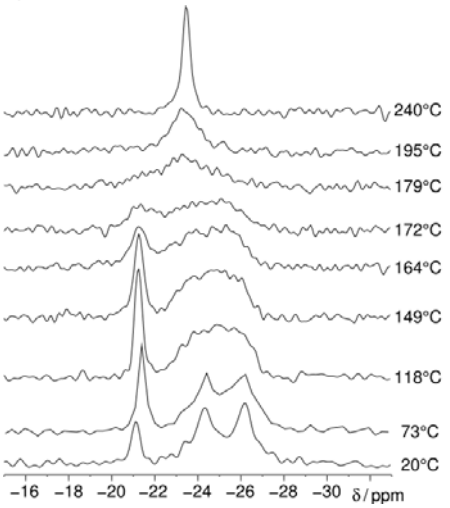

Figure 4. Isotropic peaks in a $^{31}P\{^1H\}$ CP-RAMP MAS NMR spectrum of $[N(CH_3)_4]_2HP_3O_9$ at different temperatures during heating (spinning frequency 3 kHz, complete spectra Figure S6).

During heating three different signals merge into a single broad signal with an average chemical shift. At approximately 180 °C a single broad signal can be observed caused by coalescence. Within the high temperature phase γ the phosphorus atoms cannot longer be distinguished, so that only one sharp signal can be observed (Figure 4). The cooling behavior can be viewed in Figures S5 and S7.

^{31}P MAS NMR spectra were simulated in order to find out whether the observed changes in line width and the apparent merging of the resonances observed in the experimental spectra at high temperature are consistent with a stochastic rotational motion of the cyclotriphosphate ion. The simulation takes into account only the chemical shift as dominating interaction but neglects through-space and through-bond dipolar interactions. An input to these simulations is the orientation of the chemical shift tensors, which were estimated from quantum chemical calculations (Figure S8), while the principle values were taken from experimental data (Table 1). An important insight which the quantum chemical calculations convey is that the three sites share an approximately common direction for δ_{zz} when taking the crystal structure as a reference for our simulations. Consequently the rotational motion reduces the chemical shift anisotropy δ_{aniso} only slightly (Table 1). The expected change becomes obvious from the calculated second moments M_2 of the total line shape of all peaks and their spinning sidebands as shown in Figure S9. Experiment and simulation show in a good agreement only a minor reduction of M_2 of a few per cent. From the simulations it becomes clear that the experimental data lack points in the coalescence regime which is due to the rather limited temperature resolution of the LASER MAS probe head. In view of the fairly high activation energy this is to be expected (see below). We conclude that the observed changes of the line shape are in full agreement with a rotational stochastic motion of the cyclotriphosphate anion, which is a necessary prerequisite to the paddle wheel mechanism.

Obviously such a rotational motion is not possible if the protons would remain immobile. We thus further try to estimate activation energies for the rotational cyclotriphosphate motion and the proton dynamics.

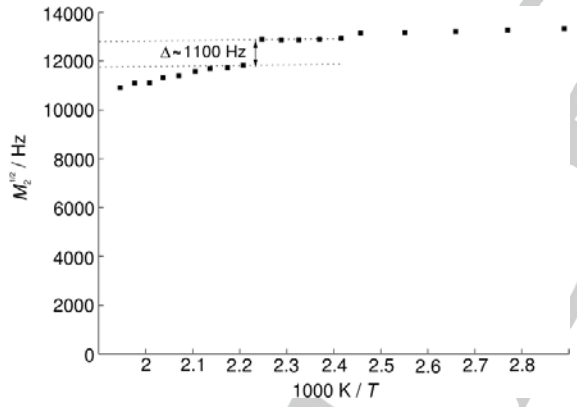

Figure 5. Plot of second moments $M_2^{1/2}$ of the complete ^{31}P MAS NMR line shape (including spinning sidebands) of $[N(CH_3)_4]_2HP_3O_9$ at various reciprocal temperatures.

The activation energies for the rotational cyclotriphosphate motion can be estimated from the onset of the reduction of the second moment M_2 of the complete line shape with rising temperatures. We assign the reduction in the square root of the second moment in between 172 and 179 °C (Figure 5) of about 1100 Hz to the stochastic rotational motion of the cyclotriphosphate because the already mentioned quantum dynamic simulations show a similar reduction (Figure S10). The activation energy for this process can be estimated with the empirical expression $E_A \approx 1.617 \cdot 10^{-3} T_{onset}$ eV / K by Waugh and Fedin[25] with an error of approximately 10 % which translates to an activation energy of approximately 0.73±0.08 eV.

Additionally we note a minor reduction of 200 Hz between 134 and 141 °C which could be attributed to a vibrational mode of the cyclotriphosphate. The estimation for the activation energy for this process results in 0.66±0.08 eV.

A second independent approximation of the activation energy can be obtained from the second moment of an individual spinning sideband in the high temperature, fast exchange regime. For this regime it has been shown that τ_c and the line width are proportional to one another.[26,27] Assuming an Arrhenius behavior for the correlation time as devised by a theory put forward by Bloembergen, Purcell and Pound (BPP) the activation energy can be determined from the slope in a logarithmic plot of line width or square root of the second moment vs. inverse temperature to a value of 0.6±0.1 eV (Figure 6).[28,29] This is in good agreement with the values obtained by estimation via Waugh and Fedin.

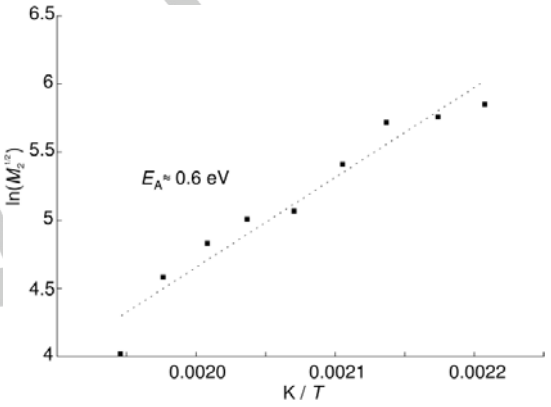

Figure 6. Arrhenius plot of the natural logarithm of the second moment $M_2^{1/2}$ of the ^{31}P MAS NMR line shape of an individual spinning sideband versus reciprocal temperature.

Finally AC impedance spectra were measured to determine the bulk ion conductivity. The ionic conductivity was characterized by means of impedance spectroscopy over a broad frequency range and at temperatures from 100 to 250 °C.

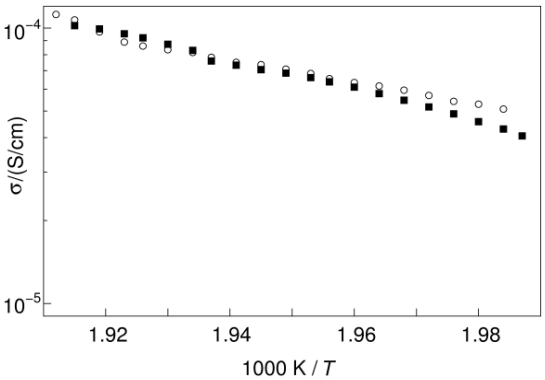

Figure 7. Logarithmic plot of proton conductivities of γ-$N(CH_3)_4]_2HP_3O_9$ for a single run between 230 and 250 °C. Filled squares: heating; empty circles: cooling; consecutive runs of heating and cooling cycles (not shown) show a minor improvement of the proton conductivity, which could be explained by a compaction of the material in the measurement cell.

Within the complete temperature range from 230 to 250 °C the temperature dependence of the conductivity (Figure 7) can be well described by an Arrhenius law: $\sigma = A \cdot \exp(-E_A / k_B T)$. The obtained value for the conductivity at 240 °C is $6.9 \cdot 10^{-5}$ S/cm with an activation energy of 1.0 ± 0.1 eV. This value is slightly higher than the values for the activation energy determined by BPP-theory or by Waugh- and Fedin-estimation. This can be explained by a higher activation energy for the bulk material than for the molecular activation energies.

In conclusion, we have demonstrated that fast dynamics of the cyclotriphosphate ion at elevated temperatures are accompanied by increased protonic conductivity. The activation energies of both processes are of similar magnitude which agrees with the paddle-wheel mechanism. Tetramethylammonium proved to be a viable (supersized) alternative to monovalent inorganic cations and allowed us to prove the rotational motion of cyclotriphosphate in a crystalline solid for the first time.

Keywords: NMR spectroscopy • ion conductor • second moment analysis • phase transition • paddle wheel

[1] G. Alberti, M. Casciola, *Solid State Ion.* **2001**, *145*, 3–16.
[2] K.-D. Kreuer, S. J. Paddison, E. Spohr, M. Schuster, *Chem. Rev.* **2004**, *104*, 4637–4678.
[3] T. Norby, *Solid State Ion.* **1999**, *125*, 1–11.
[4] J. W. Phair, S. P. S. Badwal, *Ionics* **2006**, *12*, 103–115.
[5] D. A. Boysen, S. M. Haile, H. Liu, R. A. Secco, *Chem. Mater.* **2004**, *16*, 693–697.
[6] S. M. Haile, C. R. I. Chisholm, K. Sasaki, D. A. Boysen, T. Uda, *Faraday Discuss.* **2006**, *134*, 17–39.
[7] R. Baies, V. Pralong, V. Caignaert, M. P. Saradhi, U. V. Varadaraju, B. Raveau, *Inorg. Chem.* **2008**, *47*, 6072–6076.
[8] G. Alberti, M. Casciola, U. Costantino, M. Leonardi, *Solid State Ion.* **1984**, *14*, 89–295.
[9] G. Alberti, M. Casciola, L. Massinelli, R. Palombari, *Ionics* **1996**, *2*, 179–183.
[10] K.-D. Kreuer, *J. Membr. Sci.* **2001**, *185*, 29–39.
[11] K. Fujita, D. R. MacFarlane, K. Noguchi, H. Ohno, *Acta Crystallogr. Sect. E Struct. Rep. Online* **2009**, *65*, o797–o797.
[12] N. Ohama, M. Machida, T. Nakamura, Y. Kunifuji, *Acta Crystallogr. C* **1987**, *43*, 962–964.
[13] M. Mangstl, V. R. Celinski, S. Johansson, J. Weber, F. An, J. Schmedt auf der Günne, *Dalton Trans* **2014**, *43*, 10033–10039.
[14] M. Mangstl, V. R. Celinski, C. Pritzel, R. Trettin, J. Schmedt auf der Günne, *Z. Anorg. Allg. Chem.* **2017**, *643*, 1609–1614.
[15] E. A. Secco, *Solid State Ion.* **1988**, *28*, 168–172.
[16] E. A. Secco, *J. Solid State Chem.* **1992**, *96*, 366–375.
[17] A. Lundén, *Solid State Ion.* **1988**, *28*, 163–167.
[18] D. Wilmer, R. D. Banhatti, J. Fitter, K. Funke, M. Jansen, G. Korus, R. E. Lechner, *Phys. B Condens. Matter* **1997**, *241*, 338–340.
[19] G. Kim, J. M. Griffin, F. Blanc, S. M. Haile, C. P. Grey, *J. Am. Chem. Soc.* **2015**, *137*, 3867–3876.
[20] J. R. Gardinier, P. J. Pellechia, M. D. Smith, *J. Am. Chem. Soc.* **2005**, *127*, 12448–12449.
[21] G. S. Kottas, L. I. Clarke, D. Horinek, J. Michl, *Chem. Rev.* **2005**, *105*, 1281–1376.
[22] V. Balzani, A. Credi, M. Venturi, *Molecular Devices and Machines A Journey into the Nanoworld*, Wiley-VCH, Weinheim, **2006**.
[23] V. Favre-Nicolin, R. Cherny, *J. Appl. Crystallogr.* **2002**, *35*, 734.
[24] M. Bak, J. T. Rasmussen, N. C. Nielsen, *J. Magn. Reson.* **2000**, *147*, 296–330.
[25] J. S. Waugh, E. I. Fedin, *Sov. Phys. - Solid State* **1963**, *4*, 1633–1636.
[26] K. C. Ramey, D. J. Louick, P. W. Whitehurst, W. B. Wise, R. Mukherjee, R. M. Moriarty, *Org. Magn. Reson.* **1971**, *3*, 201–216.
[27] W. Hoffbauer, S. Wefing, G. Klösters, F. Frick, M. Jansen, *Solid State Nucl. Magn. Reson.* **1999**, *14*, 211–224.
[28] N. Bloembergen, E. M. Purcell, R. V. Pound, *Phys. Rev.* **1948**, *73*, 679.
[29] A. Schmidt, S. Vega, *J. Chem. Phys.* **1987**, *87*, 6895–6907.